

The Effect of Directivity-Induced Pulse-Like Ground Motions on Fracture Risk of Welded Steel Column Splices

Biao Song

PhD Student, Department of Civil, Environmental & Geomatic Engineering, University College London, London, United Kingdom

Carmine Galasso

Associate Professor, Department of Civil, Environmental & Geomatic Engineering, University College London, London, United Kingdom

ABSTRACT: Recent, worldwide earthquakes have highlighted the destructive potential of near-fault, pulse-like ground motions caused by forward directivity. This study investigates the fracture risk of welded steel column splices (WCSs) in near-fault regions, especially quantifying the pulse effects on WCS stress demands through incremental dynamic analysis (IDA). For this purpose, two case-study nonlinear steel moment frame models are developed and subjected to a set of pulse-like ground motions with varying pulse periods and a suite of ordinary (i.e., non-pulse-like) ground motions, respectively. Results of IDA are then combined with near-source probabilistic seismic hazard analysis (NS-PSHA) to assess fracture risk. Findings from the study suggest that WCSs in pre-Northridge steel frames may be highly susceptible to fracture due to directivity-induced pulse-like ground motions.

1. INTRODUCTION

In near-fault regions, ground motions can be often characterized by a large-amplitude and long-duration pulse in the first portion of the ground velocity time history; such a pulse mainly occurs in the fault-normal direction. These pulse-like ground motions are caused primarily by forward directivity (e.g., Shahi and Baker 2011): when the fault rupture propagates towards the site and the rupture velocity is close to the shear-wave velocity, a high-amplitude pulse can be generated due to the constructive interference between the arrival of the seismic energy from the rupture and the seismic wave front (Somerville et al. 1997). Such a pulse has an occurrence probability that depends upon the site-to-source geometry, earthquake magnitude, and other characteristics (e.g., Iervolino and Cornell 2008). Hence, these directivity-induced pulse-like ground motions recorded close to a fault rupture are distinct from the ordinary (i.e., non-pulse-like) ground motions.

In several near-fault regions, particularly in the west coast of the United States, welded steel

moment frames (WSMFs) are the primary lateral load resisting systems for earthquake resistance. Within mid- to high-rise WSMF structures, welded column splices (WCSs) are commonly used to manage length/transportation constraints and/or downsizing of the column sections due to the changes in loading at higher stories of the structure (Shaw et al. 2015). Recent studies by the authors (e.g., Galasso et al. 2015) have shown that the fracture risk of pre-Northridge WCSs subjected to ordinary ground motions is relatively high due to three main issues: (1) they utilized low toughness welds, resulting in significantly low fracture strength; (2) they featured partial joint penetrations (PJP), producing a cracklike flaw in the region of low material toughness (i.e., unfused weld root); (3) they are force-controlled and their fracture is dominated by the tensile stress (rather than the inelastic deformation).

The higher structural risk due to near-fault, pulse-like ground motions compared with far-fault ordinary ground motions has been highlighted by several recent earthquakes (e.g., Chioccarelli and

Iervolino 2010). In the available literature published so far, most comparisons of structural responses subjected to pulse-like and ordinary earthquake records have focused on the global deformation at (or near) the collapse limit state (e.g., Champion and Liel 2012). To the author's knowledge, local engineering demand parameters (EDPs), such as the stress demand (denoted as σ_D , controlling the fracture of WCSs), have not been properly investigated and quantified in the case of pulse-like ground motion records.

Consequently, this study further investigates the fracture risk of WCSs in near-fault regions, particularly addressing the effect of forward directivity and pulse-like ground motions on the distribution of splice stress demands.

2. BUILDING MODELS AND GROUND MOTION SETS

2.1. Nonlinear case-study models

To characterize the stress demand of WCSs, two generic steel moment resisting frames (i.e., 4- and 20-story) are simulated in this study using OpenSees (Mazzoni et al. 2009). Figure 1 schematically shows the frames and the locations of the WCSs (indicated by block arrows). Both frames are identical to those used by Shaw et al. (2015) and Galasso et al. (2015). The fundamental periods (denoted as T_1) of these two frames are 0.94 and 2.36 s, respectively. Further details of the building design and modelling approaches can be found in Shaw (2013) and Shaw et al. (2015).

2.2. Ground motion datasets

Two sets of ground motions (i.e., pulse-like and ordinary records) are utilized. First, a set of 91 pulse-like ground motions is employed for nonlinear dynamic analysis. These ground motions were identified by Baker (2007) from the Next Generation Attenuation (NGA) database of the Pacific Earthquake Engineering Research (PEER) Center. All the records in this set have been rotated to the fault-normal direction and have pulse periods (denoted as T_p) ranging from 0.4 to 12.9 s. The full list of this set can be found in Baker (2007).

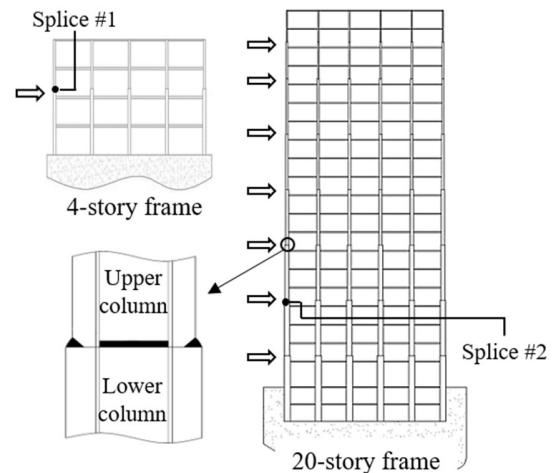


Figure 1: Schematic illustration of 4-story and 20-story steel frame models and welded column splice

A second set of records is used in this study to represent the far-field, ordinary ground motions. They were collected from the Federal Emergency Management Agency (FEMA) P695 far-field record set (Applied Technology Council 2009), which contains 22 record pairs, each with two horizontal components (i.e., 44 records in total). Initially, nine of these records were removed from the considered set, because they exhibit pulses in velocity time history based on the wavelet classification algorithm results (Champion and Liel 2012). Moreover, for each pair of ground motions, only the component characterized by the larger peak ground acceleration value was arbitrarily selected to reduce the computational burden (yet maintaining a statistically significant number of records for the analysis). Finally, a set of 21 records is used to represent generic far-field, ordinary ground motions in this study. The selected far-field ground motion set used here is structure-type (i.e., period) and site-hazard independent as no specific spectral shape (and corresponding period range) was considered in record selection.

3. FRACTURE EVALUATION APPROACH

The seismic fracture risk of each case-study frame is evaluated through IDA (Vamvatsikos and Cornell 2002). According to IDA, each building model is subjected to the ground motion record described in Section 2.2, for far-field ordinary and

near-fault pulse-like sets, respectively. Each input ground motion is linearly scaled to increasing intensity levels until fracture occurs. This analysis is repeated for both structural models, and for all the selected earthquake records. The considered seismic intensity measure (IM) in this study is the spectral acceleration at the fundamental period of each frame, denoted as $S_a(T_1)$ (simply S_a hereinafter). The monitored response parameter (i.e., EDP) is the peak tensile stress (σ_D) obtained from the flange of selected splice. The occurrence of fracture is considered when σ_D exceeds the stress capacity (denoted as σ_C) for the splice of interest. In particular, two representative splices (i.e., splice #1 and splice #2 of 4- and 20-story frames, indicated in Figure 1), have been selected, using a similar approach to that of Galasso et al. (2015).

To determine σ_C , a fracture-mechanics-based approach proposed by Stillmaker et al. (2016) is adopted. Particularly, the stress capacity of WCS is a function of initial crack length (a), upper and lower flange thickness of WCS (t_{upper} and t_{lower}) and the fracture toughness of welded material (e.g., Charpy V-Notch, CVN, value). The nominal values of flange thicknesses of splice #1 and #2 are given in Shaw (2013). For the pre-Northridge era, the initial crack length of WCS is assumed as half of t_{upper} (Bruneau and Mahin 1990) and the typical value of CVN toughness is assigned as 13.6 J (Chi et al. 2000). Following these specifications, the mean (deterministic) values of fracture strength for splice #1 (4-story) and #2 (20-story) are calculated as 111.7 and 108.2 MPa, respectively.

Additionally, the maximum peak inter-story drift ratio (denoted as MIDR) is also recorded for each model in IDA. All the observed results show that the fracture criterion (i.e., $\sigma_D > \sigma_C$) is always violated at the lower S_a level, before MIDR reaches a conventional 10%-threshold for global collapse (or any numerical dynamic instability is noted).

3.1. Fracture evaluation under far-field records

Based on the results of IDA subjected to far-field ordinary earthquake record set, the proportion of ground motions at each S_a level causing fracture on the total number record can be computed. To derive fracture fragility curves, the maximum likelihood

approach is used (Baker 2015). The determined median value and the lognormal standard deviation (denoted as β) of the S_a intensities at which fracture occurs fully define the obtained fracture fragility function.

As mentioned in Section 2.2, the far-field ground motion set was selected without any consideration of spectral shape. To measure the distinct spectral shape of a ground motion, the parameter epsilon (denoted as ϵ), which is defined as the number of logarithmic standard deviations between the observed spectral value (of used record) and the mean value estimated from ground motion prediction equations (GMPEs) for a specified structural period, earthquake magnitude, fault condition, and site-to-source distance, has been introduced (Baker and Cornell 2005).

In this study, the resulting fracture fragility curves for ordinary ground motions have been adjusted to consider the effect of spectral shape (ϵ) using the simplified method proposed by Haselton et al. (2011). The GMPE developed by Boore and Atkinson (2008) is adopted here. An example of such an adjustment of ϵ for the fracture fragility curves of the 4-story frame ($T_1 = 0.94$ s) is shown in Figure 2, assuming a far-field strike-slip (SS) earthquake with moment magnitude $M_w = 7$, closest distance $R = 50$ km, and a value of averaged shear wave velocity over top 30 m (denoted as $V_{s,30}$) as 800 m/s. This scenario has been chosen to provide a fair comparison with the pulse-like case, as discussed in the following sub-section.

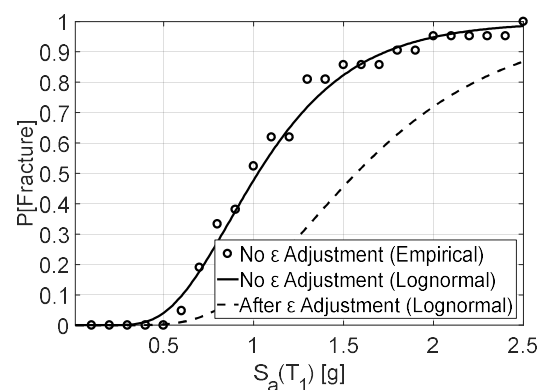


Figure 2: An example of ϵ adjustment for fracture fragility curves subjected to far-field ground motions

3.2. Effect of velocity pulse on fracture analysis

For the near-fault pulse-like ground motions, the probability of fracture depends not only on $S_a(T_1)$, but also on the pulse period (T_p) of the record. Unlike the far-field records, it is assumed that the scaling of pulse-like ground motions does not introduce significant biases on fracture fragility assessment, if both T_p and $S_a(T_1)$ are accounted for. A similar finding is discussed in Champion and Liel (2012). Therefore, several bins of pulse-like ground motions with different T_p values should be considered, to investigate the influence of T_p and eliminate the effect of ε on the predicted fracture capacity.

Figure 3 plots the ratio of T_p to T_1 versus the fracture capacity for the 4-story steel frame. The fracture capacity of each pulse-like record was obtained from the corresponding IDA results by interpolating between two S_a levels, within which the estimated σ_D exceeds σ_C . The larger fracture capacity means that the ground motion was scaled to higher S_a level before fracture occurs. Moreover, the moving average of the empirical data is also plotted in Figure 3. This is computed by averaging the point of interest with five previous and subsequent data points. Similar trend is observed for the 20-story frame considered in this study (not shown for the sake of brevity). Based on the shape of moving average curve, the dependence of fracture $S_a(T_1)$ values resulting from varying T_p can be observed.

According to the moving average curve in Figure 3, the highest values of fracture $S_a(T_1)$ are obtained in the region where the pulse period (T_p) is approximately equal to the fundamental period of structure (T_1). This observation indicates that the frame is least susceptible to seismic fracture when $T_p \approx T_1$, which is inconsistent with the response of linear-elastic system. However, it may be explained by (1) contribution of higher modes to the structural response, particularly in terms of stresses; and (2) elongation of the effective period due to the building inelastic response. Consequently, the pulse-like ground motions with $T_p < T_1$ and $T_p > T_1$ are more critical in terms of seismic fracture.

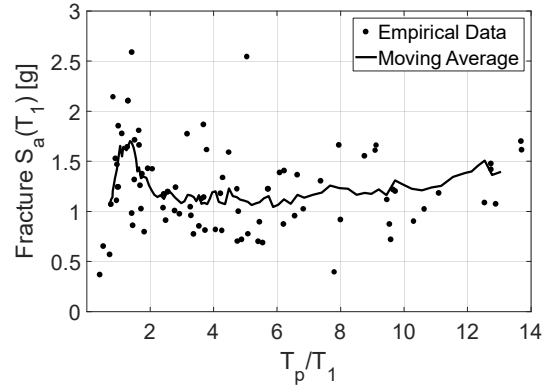


Figure 3: Relationship between fracture $S_a(T_1)$ of 4-story frame and T_p/T_1 ratio of 91 pulse-like records

4. FRACTURE RISK ASSESSMENT INCLUDING NEAR-FAULT DIRECTIVITY

As explained in Section 3, structural fracture capacity at a near-fault site depends on both $S_a(T_1)$ and the occurrence of a velocity pulse (with its associated T_p). By using the total probability theorem, the probability of fracture (recall the fracture criterion, i.e., $\sigma_D > \sigma_C$) including the effects of near-fault directivity, $P[\text{Fracture}|S_a = x]$, for a given $S_a(T_1)$ value, can be expressed as

$$\begin{aligned} & P[\text{Fracture}|S_a = x] \\ &= P[\text{Fracture}|S_a = x, \text{Pulse}] \cdot P[\text{Pulse}|S_a = x] \\ &+ P[\text{Fracture}|S_a = x, \text{No Pulse}] \cdot P[\text{No Pulse}|S_a = x] \end{aligned} \quad (1)$$

The expression $P[\text{Fracture}|S_a = x, \text{No Pulse}]$ is the probability of fracture for no-pulse records, and can be determined directly from the fracture fragility curves constructed for far-field ordinary ground motions (after the adjustment for ε , Section 3.1). The probability of fracture for pulse-like records, $P[\text{Fracture}|S_a = x, \text{Pulse}]$, depends on the pulse period and the corresponding distribution of pulse periods at the specific S_a level:

$$\begin{aligned} & P[\text{Fracture}|S_a = x, \text{Pulse}] \\ &= \sum_{i=1}^{\text{All } T_p} P[\text{Fracture}|T_p = t_i, S_a = x, \text{Pulse}] \\ &\quad \cdot P[T_p = t_i|S_a = x, \text{Pulse}] \end{aligned} \quad (2)$$

The probability of fracture for each given T_p value, $P[\text{Fracture}|T_p = t_i, S_a = x, \text{Pulse}]$, is obtained from the relevant moving average curve plotted for each building (e.g., Figure 3, Section 3.2). The values determined from the curve are assumed to represent the median (lognormal mean) of the fracture $S_a(T_I)$ as a function of T_p . Then, a lognormal distribution (with the median just obtained at a given T_p and a lognormal standard deviation) can be defined to compute the probability of fracture for the given T_p . This lognormal standard deviation is assumed to be equal to the corresponding β estimated from IDA results for $P[\text{Fracture}|S_a = x, \text{No Pulse}]$.

In order to determine the other terms in Eqs. (1) and (2), near-source probabilistic seismic hazard analysis (NS-PSHA, e.g., Shahi and Baker 2011) should be performed. NS-PSHA is used to compute the mean annual frequency (MAF) of exceeding a spectral intensity (denoted as $\lambda_{S_a > x}$), accounting for potential near-fault directivity. For a single seismic fault, $\lambda_{S_a > x}$ is generally defined as

$$\lambda_{S_a > x} = v \int \int \int P[S_a > x | m, r, z] \cdot f_{M,R,Z}(m, r, z) dm dr dz \quad (3)$$

where, v is the mean annual rate of earthquake occurrence on the fault, M is the earthquake magnitude, R is the site-to-source distance, Z defines the site-to-source geometry, and $f_{M,R,Z}$ is the joint probability density function of M , R and Z . The term $P[S_a > x | m, r, z]$ is the probability that a specific S_a value is exceeded, it depends on the probability of pulse occurrence, the distribution of possible pulse periods, and the peculiar spectral shape caused by the pulse.

In this study, the model of Iervolino and Cornell (2008) is selected to compute the probability of a pulse occurring, $P[\text{Pulse}]$. The pulse period distribution model employed here was determined by Chioccarelli and Iervolino (2010), and expressed as a function of earthquake magnitude. To capture the spectral shape induced by the pulse, a modifying factor suggested in Baker (2008) is applied to the original GMPE used in this study (i.e., Boore and Atkinson 2008).

To allow the combination with the fracture fragility curves described in Eq. (1), the NS-PSHA should be represented as $\lambda_{S_a = x}$, rather than $\lambda_{S_a > x}$, because the MAF of a given S_a is of interest. Once $\lambda_{S_a = x}$ has been calculated, hazard disaggregation can be performed to compute the probability of pulse occurrence at the S_a level:

$$P[\text{Pulse}|S_a = x] = \lambda_{S_a = x, \text{Pulse}} / \lambda_{S_a = x} \quad (4)$$

According to Eq. (4), $P[\text{Pulse}|S_a = x]$ is defined as the ratio of the MAF of $S_a = x$ when only pulse-like records are considered to the total MAF of $S_a = x$. Note that this hazard disaggregation is required for all the considered S_a levels. Following this, the term $P[\text{No Pulse}|S_a = x]$ is given as:

$$P[\text{No Pulse}|S_a = x] = 1 - P[\text{Pulse}|S_a = x] \quad (5)$$

Similarly, the term $P[T_p = t_i | S_a = x, \text{Pulse}]$ (i.e., the marginal disaggregation distribution of pulse period) can also be computed by considering only the case of pulse occurrence (Chioccarelli and Iervolino 2013).

4.1. Description of near-fault sites

In this study, a single characteristic M7 strike-slip fault is assumed to compare the seismic fracture risk of WCS steel frames located at near-fault sites and far-field sites. Based on mean value of the Wells and Coppersmith (1994) magnitude-scaling relation, the length of this fault is 42 km. The mean annual rate of earthquake occurrence on the fault (v) is assumed as 0.05 and the location of earthquake epicenters is uniformly distributed along the fault. As shown in Figure 4, six sites with site-to-source distance of 5, 10 and 15 km at the end (i.e., “end-of-fault” sites) and midpoint (i.e., “midfault” sites) are considered. Based on the assumed single fault and the representative sites, results of NS-PSHA for the 4-story frame ($T_I = 0.94$ s) are also shown in Figure 4, together with the hazard disaggregation results in terms of $P[\text{Pulse}|S_a = x]$ for the same frame.

4.2. Results and discussion

IDA results (Section 3) for the case-study steel frames are used to assess the potential increase in

seismic fracture risk due to the effects of near-fault directivity. Applying the probabilistic methods explained in Section 4, the fracture fragility curves of both frames at all near-fault sites are developed (e.g., Figure 5 for the 4-story frame) and the corresponding median fracture capacity results are listed in Table 1.

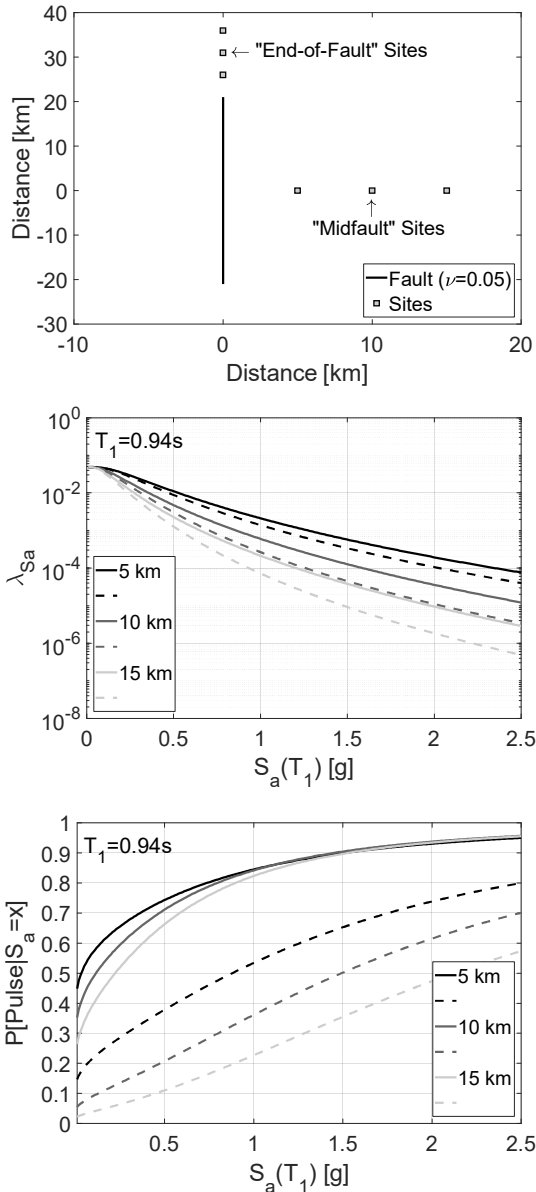


Figure 4: Representative near-fault sites considered, showing site locations (top); results of seismic hazard curves (middle) and probabilities of pulse occurrence (bottom) for 4-story frame ($T_1 = 0.94$ s) at midfault (dashed lines) and end-of-fault (solid lines) sites

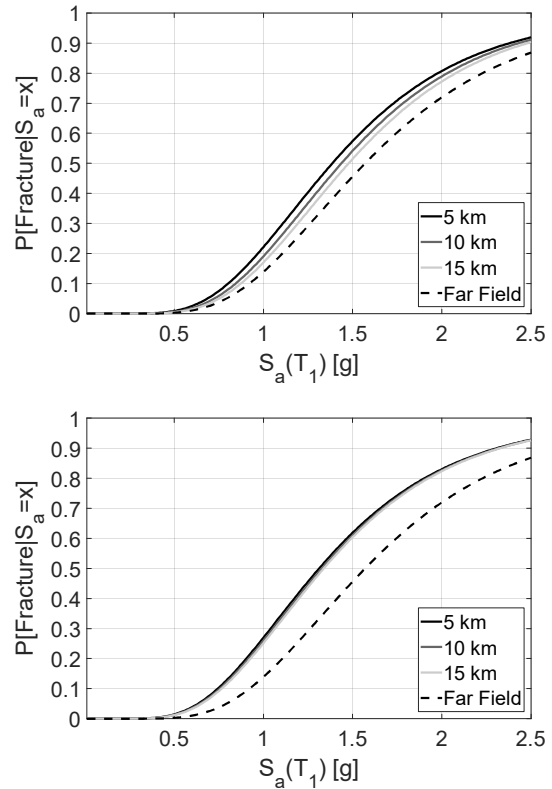


Figure 5: Fracture fragility functions for 4-story frame at three different midfault (top) and end-of-fault (bottom) sites, with far-field fragility curves

Table 1: Median fracture capacity, $S_a(T_1)$ [g]

Frame	Midfault sites			End-of-fault sites		
	5km	10km	15km	5km	10km	15km
4-story	1.386	1.437	1.478	1.313	1.327	1.338
20-story	0.242	0.244	0.246	0.237	0.238	0.238

The impact of site-to-source distance on the probability of fracture is illustrated in Figure 5 for the 4-story frame. The higher probabilities of fracture for sites closer to the fault are observed. The far-field fragility curves are also plotted in the same figures for comparison. In the case of 4-story frame, the pulse effects can reduce the median fracture capacity more than 15%. As can be seen from Figure 5 and Table 1, the differences of the fracture fragility curves and their median fracture capacities at three end-of-fault sites are moderate, because, referring to Figure 4, the pulse probabilities (for each S_a level) at these three sites are similar. Conversely, considerable separations

can be found in the fracture fragility curves (and the fracture capacities) at midfault sites, due to the larger differences in pulse probabilities, such that shown in Figure 4.

Additionally, the probability of fracture in 50 years, $P[\text{Fracture in 50 years}]$, is also calculated to directly show the fracture risk of WCS at near-fault sites. A Poisson distribution of earthquake occurrences is assumed to compute this:

$$P[\text{Fracture in 50 years}] = 1 - e^{-\lambda[\text{Fracture}]t} \quad (6)$$

where, t is the time in years and $\lambda[\text{Fracture}]$ is the MAF of fracture, written as:

$$\lambda[\text{Fracture}] = \sum_{\text{all } x_i} P[\text{Fracture} | S_a = x_i] \cdot |\Delta\lambda_{S_a}(x_i)| \quad (7)$$

where, $P[\text{Fracture}|S_a = x_i]$ can be obtained from fracture fragility curves and $|\Delta\lambda_{S_a}(x_i)|$ is the MAF of exceeding for each S_a value. The results of such calculations are presented in Table 2. As expected, fracture risk at near-fault sites decreases with the increase of the site-to-source distance, indicating a large increase in the fracture risk of WCS due to near-fault directivity.

Table 2: Probability of fracture in 50 years [%]

Frame	Midfault sites			End-of-fault sites		
	5km	10km	15km	5km	10km	15km
4-story	4.90	1.01	0.29	8.26	2.76	1.10
20-story	30.03	12.07	5.16	41.58	25.75	15.22

Comparing the fracture risk at each of the midfault and end-of-fault sites for the same frame, the larger values of fracture probability are found at the end-of-fault sites. This is mainly because the probabilities of pulse-like ground motions occurrence, which depend on the site-to-source geometry, are higher at the end-of-fault sites (refer to Figure 4). The rupture directivity is towards these sites, in terms of the geometry (Shahi and Baker 2011). Also, the fracture risk is largely affected by the site location with respect to the fault axis, compared with the effects caused by the site-to-source distance.

5. CONCLUSIONS

This study investigated the effects of near-fault directivity on fracture risk of welded steel column splices, through nonlinear dynamic analysis of two case-study frames (i.e., 4-story and 20-story, respectively). A suite of 91 near-fault, pulse-like ground motions and a set of 21 far-field, ordinary records were used to conduct IDA. The results of IDA were combined with NS-PSHA to evaluate the fracture risk including pulse effects at six different near-fault sites.

Based on IDA results of pulse-like records, the seismic fracture of WCSs in the near-fault region is mainly controlled by the ratio between pulse period of a ground motion and fundamental period of the assessed structure (i.e., T_p/T_1). The probabilistic fracture risk assessment results, in terms of the fragility curves and the probability of fracture in 50 years (derived from MAF of fracture), indicate that the fracture risk experiences a considerable increase, when the near-fault directivity is properly accounted in the PSHA and the structural response simulation. In particular, the fracture risk of WCS substantially increases as the site-to-source distance decreases. However, considering any specific frame, the influence of the distance from fault rupture on the fracture risk is less significant to the effect caused by the relative site location to the fault axis.

6. ACKNOWLEDGEMENT

The first author would like to acknowledge the financial support from China Scholarship Council (CSC) and University College London (UCL) through a joint research scholarship.

7. REFERENCES

- Applied Technology Council. (2009). *Quantification of Building Seismic Performance Factors (FEMA P695)*. Redwood City, CA.
- Baker, J. W. (2007). "Quantitative Classification of Near-Fault Ground Motions Using Wavelet Analysis." *Bulletin of the Seismological Society of America*, 97(5), 1486–1501.
- Baker, J. W. (2008). "Identification of near-fault velocity pulses and prediction of resulting response spectra." *Geotechnical Earthquake Engineering and Soil Dynamics IV*, Sacramento,

- CA.
- Baker, J. W. (2015). "Efficient Analytical Fragility Function Fitting Using Dynamic Structural Analysis." *Earthquake Spectra*, 31(1), 579–599.
- Baker, J. W., and Cornell, C. A. (2005). "A vector-valued ground motion intensity measure consisting of spectral acceleration and epsilon." *Earthquake Engineering & Structural Dynamics*, 34(10), 1193–1217.
- Boore, D. M., and Atkinson, G. M. (2008). "Ground-Motion Prediction Equations for the Average Horizontal Component of PGA, PGV, and 5%-Damped PSA at Spectral Periods between 0.01 s and 10.0 s." *Earthquake Spectra*, 24(1), 99–138.
- Bruneau, M., and Mahin, S. A. (1990). "Ultimate Behavior of Heavy Steel Section Welded Splices and Design Implications." *Journal of Structural Engineering*, 116(8), 2214–2235.
- Champion, C., and Liel, A. (2012). "The effect of near-fault directivity on building seismic collapse risk." *Earthquake Engineering & Structural Dynamics*, 41(10), 1391–1409.
- Chi, W.-M., Deierlein, G. G., and Ingrassia, A. (2000). "Fracture Toughness Demands in Welded Beam-Column Moment Connections." *Journal of Structural Engineering*, 126(1), 88–97.
- Chioccarelli, E., and Iervolino, I. (2010). "Near-source seismic demand and pulse-like records: A discussion for L'Aquila earthquake." *Earthquake Engineering & Structural Dynamics*, 13(9), 1039–1062.
- Chioccarelli, E., and Iervolino, I. (2013). "Near-source seismic hazard and design scenarios." *Earthquake Engineering & Structural Dynamics*, 42(4), 603–622.
- Galasso, C., Stillmaker, K., Eltit, C., and Kanvinde, A. (2015). "Probabilistic demand and fragility assessment of welded column splices in steel moment frames." *Earthquake Engineering & Structural Dynamics*, 44(11), 1823–1840.
- Haselton, C. B., Baker, J. W., Liel, A. B., and Deierlein, G. G. (2011). "Accounting for Ground-Motion Spectral Shape Characteristics in Structural Collapse Assessment through an Adjustment for Epsilon." *Journal of Structural Engineering*, 137(3), 332–344.
- Iervolino, I., and Cornell, C. A. (2008). "Probability of Occurrence of Velocity Pulses in Near-Source Ground Motions." *Bulletin of the Seismological Society of America*, 98(5), 2262–2277.
- Mazzoni, S., McKenna, F., Scott, M. H., and Fenves, G. L. (2009). *Open System for Earthquake Engineering Simulation User Command-Language Manual. OpenSees version 2.0*. Pacific Earthquake Engineering Research Center, University of California, Berkeley, Berkeley, CA.
- Shahi, S. K., and Baker, J. W. (2011). "An Empirically Calibrated Framework for Including the Effects of Near-Fault Directivity in Probabilistic Seismic Hazard Analysis." *Bulletin of the Seismological Society of America*, 101(2), 742–755.
- Shaw, S. M. (2013). "Seismic Performance of Partial Joint Penetration Welds in Special Moment Resisting Frames. PhD Thesis." University of California, Davis.
- Shaw, S. M., Stillmaker, K., and Kanvinde, A. M. (2015). "Seismic response of partial-joint-penetration welded column splices in moment-resisting frames." *Engineering Journal*, 52(2), 87–108.
- Somerville, P. G., Smith, N. F., Graves, R. W., and Abrahamson, N. A. (1997). "Modification of Empirical Strong Ground Motion Attenuation Relations to Include the Amplitude and Duration Effects of Rupture Directivity." *Seismological Research Letters*, 68(1), 199–222.
- Stillmaker, K., Kanvinde, A., and Galasso, C. (2016). "Fracture Mechanics-Based Design of Column Splices with Partial Joint Penetration Welds." *Journal of Structural Engineering*, 142(2), 04015115.
- Vamvatsikos, D., and Cornell, C. A. (2002). "Incremental dynamic analysis." *Earthquake Engineering & Structural Dynamics*, 31(3), 491–514.
- Wells, D. L., and Coppersmith, K. J. (1994). "New empirical relationships among magnitude, rupture length, rupture width, rupture area, and surface displacement." *Bulletin of the Seismological Society of America*, 84(4), 974–1002.